Spectral Characterization for Small Clusters of Silicon and Oxygen: SiO_2, SiO_3, Si_2O_3, & Si_2O_4

Mason B. Gardner[1], Brent R. Westbrook[1], and Ryan C. Fortenberry[1]

[1]Department of Chemistry & Biochemistry, University of Mississippi, University, MS 38677-1848

Key Points:

- Small silicon oxide clusters have bands in detectable IR ranges.
- These may be intermediates between atoms and mineral nanocrystals.
- The spectral data produced here agree well with known experimental values and extend beyond it.

Corresponding author: Ryan C. Fortenberry, r410@olemiss.edu

Abstract

Infrared spectra of evolved stars have a rise in signal between the 7.0 μm and 8.0 μm wavelengths; the antisymmetric Si−O stretches of small silicon oxide clusters fall in this range and have large intensities. Hence, this quantum chemical analysis provides data for such molecules that may be of significance for astrochemical classification and could play a role in the formation or degradation of mineral nanocrystals from or into their constituent atoms. Both explicitly computed anharmonic fundamental vibrational frequencies and those determined from scaled harmonic frequencies agree well with known experimental data, and spectroscopic constants are provided herein such that astronomical rotational spectral characterization may also be possible for the C_{2v} SiO_3 and Si_2O_3 molecules.

Plain Language Summary

Rocky bodies are made of minerals comprised largely of silicon and oxygen. How these minerals are formed from their constituent atoms is not fully known. The IR data produced in this work may help to observe small molecules containing silicon and oxygen so that these potential molecular intermediates can be observed. These molecules have strong aborption features between 7.0 μm and 8.0 μm, most notably, and are now fully characterized in the IR.

1 Introduction

Quartz, sand, and silica are all forms for the most abundant material in the Earth's crust and mantle. Crystalline SiO_2 gives way to the molten form deeper into the mantle, and it mixes with magnesium, iron, and aluminum to form most of the material present between the crust and core (White, 2013). Similar processes likely played out all over the early Solar System and even beyond since both oxygen and silicon are two of the most abundant atoms in the Universe (Savage & Sembach, 1996; McCall, 2006; Fortenberry, 2020). Consequently, there are few inorganic materials as common as silicon dioxide.

Silicon dioxide boils at nearly 3300 K and becomes isovalent with carbon dioxide in its triatomic molecular form. Such would likely be a necessary signature of silicon-based metabolism in exobiology. With regards to less exotic applications, silicates are known to condense under cold conditions creating rocky material in the first place (Rouillé et al., 2014), and these small molecules likely aggregate from silicon and oxygen atoms or the SiO monomer which has been observed in astrophysical environments since 1971 (Wilson et al., 1971). At the other end of the star's lifetime, the ablation of rocky materials as a star dies (McCarthy et al., 2019) or the stellar infall of most solid materials at any stage in a star's evolution will likely vaporize the crystalline or even molten silicates and quartzes creating small silicon oxide molecules for which little spectral data are well-known. A similar vaporization process would also take place terrestrially in foundries when high temperatures are utilized in large-scale industrial processes. Regardless of the circumstance, further spectral analysis of small silicon oxide clusters in the gas phase is necessary to produce data for the classification of silicon dioxide and its derivatives (Wang et al., 1997) such that the evolution of silicate materials from atoms to solids can be observed geophysically or industrially.

Argon matrix experiments have provided vibrational frequencies for the antisymmetric stretch and bending fundamentals of isolated SiO_2 at 1416 cm^{-1} and 273 cm^{-1}, respectively (H. Schnöckel, 1978; V. H. Schnöckel, 1980; Andrews & McCluskey, 1992; Jacox, 1994). Five of the six fundamental frequencies of SiO_3 have been tentatively assigned from similar experiments in conjunction with density functional theory analysis (DFT) (Tremblay et al., 1996), but follow-up work has not conclusively confirmed such

attributions. Most notably, the a_1 O−O stretch could not be attributed experimentally from the DFT computations. The larger structures have been observed through photoelectron spectroscopy (Wang et al., 1996, 1997), but the fundamental vibrational frequencies have not been conclusively determined in the laboratory. Three modes of Si_2O_4 have been reported in the literature again from argon matrix experiments (Mehner et al., 1980), but there has been no experimental or high-level theoretical follow-up in the intervening 30 years. Granted, the gas phase data are likely similar to the argon matrix results in each of these studies since the argon should interact far less with the silicon and oxygen atoms than they would with hydrogens, for instance, but corroboration of some variety for these modes is still lacking. While some are better understood than others, the full vibrational spectra and especially gas-phase rotational constants for each these molecules are not fully classified.

Consequently, high-accuracy spectroscopic predictions for the vibrational frequencies of these molecules will enhance spectral models of environments where they may be found both in the laboratory and in nature. Quartic force fields (QFFs) are fourth-order Taylor series approximations to the potential portion of the internuclear Hamiltonian (Fortenberry & Lee, 2019). These have been shown to produce exceptional accuracy for determining anhamronic vibrational frequencies for relatively low computational cost, provided that a sufficient electronic structure method can be used to compute this specialized potential energy surface (Fortenberry & Lee, 2019), most often coupled cluster theory at the singles, doubles, and perturbative triples [CCSD(T)](Raghavachari et al., 1989; Shavitt & Bartlett, 2009) level. The most accurate QFFs have produced vibrational frequencies to within 1 cm^{-1} on occasion and most often within 5-10 cm^{-1}. The accuracy of the rotational constants vary, but most are within 30 MHz of gas phase experiment (Huang & Lee, 2008, 2009; Huang et al., 2011; Fortenberry et al., 2011a, 2011b, 2012; Huang et al., 2013; Fortenberry et al., 2014; Zhao et al., 2014; Fortenberry et al., 2015; Kitchens & Fortenberry, 2016; Fortenberry, 2017; Bizzocchi et al., 2017).

However, the computational cost of this involved CCSD(T) approach including corrections for core electron correlation and complete basis set extrapolations is prohibitive for molecules containing more than five atoms. Recent work has shown that vibrational frequencies of closed-shell molecules utilizing explicitly correlated CCSD(T)-F12b(Adler et al., 2007; Knizia et al., 2009) for the QFF energy points are within 7 cm^{-1} of the more expensive computations and cost orders of magnitude less time (Agbaglo et al., 2019; Agbaglo & Fortenberry, 2019a, 2019b). Some CCSD(T)-F12b anharmonic vibrational frequencies are actually closer to experiment than their more costly counterparts (Agbaglo & Fortenberry, 2019a). This approach has been utilized to predict anharmonic spectral data for $MgSiO_3$ and two isomers of Mg_2SiO_4 (enstatite and forsterite monomers, respectively) for which no previous vibrational or rotational spectroscopic data, theoretical or otherwise, exist (Valencia et al., 2020). Most notably these inorganic oxides produce very large infrared intensities implying that relatively small amounts of material could still be observed (Kloska & Fortenberry, 2018; Palmer & Fortenberry, 2018; Valencia et al., 2020; Westbrook & Fortenberry, 2020). Furthermore, other studies have produced scaling factors for harmonic frequencies of small, inorganic oxides that promise to reduce the computational time further for similar species in the production of accurate, anharmonic vibrational frequencies (Westbrook & Fortenberry, 2020).

Regardless, the present work will extend the data for these geophysically- and astrochemically-relevant silicon oxides by computing the anharmonic vibrational frequencies and spectroscopic constants for four silicon oxide structures: SiO_2, SiO_3, Si_2O_3, and Si_2O_4. The D_{3h} structures of both CO_3 and SiO_3 have proven problematic in the past (Beste & Bartlett, 2002). Here, only the C_{2v} SiO_3 structure, akin to its carbon analogue which performed well in recent QFF examination (Fortenberry et al., 2019), is considered. The D_{2h} structure of Si_2O_4 has also been previously imposed to explain the results of photoelectron experiments (Wang et al., 1996) and the known vibrational frequencies thereof (Mehner

Figure 1. The optimized geometries and atom labels of A) SiO_2, B) SiO_3, C) Si_2O_3, and D) Si_2O_4.

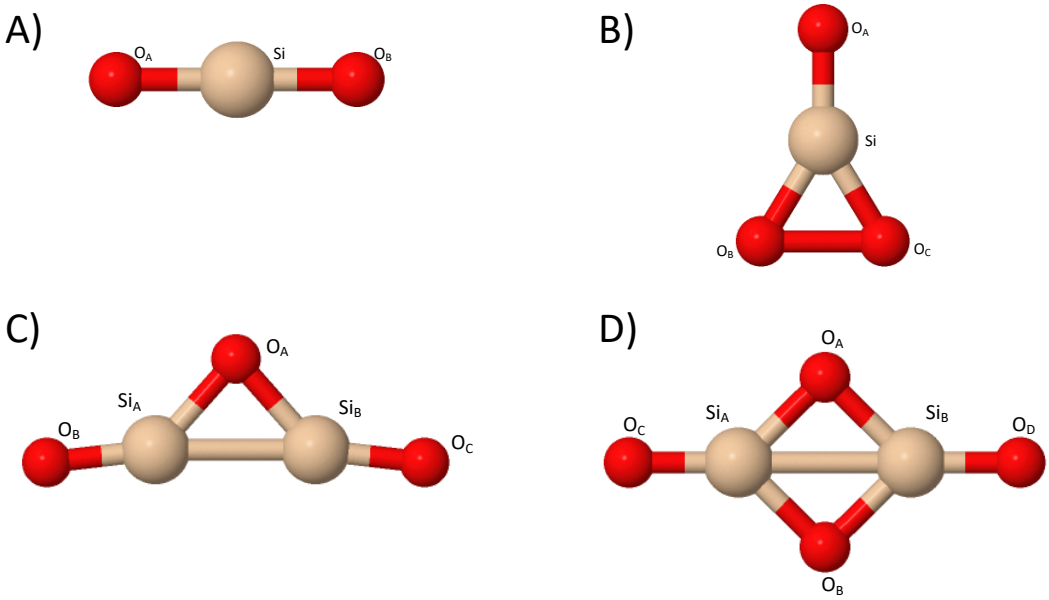

et al., 1980). The rovibrational data provided herein will help to classify the building blocks or end products of silicates in regions where the solid form is known to exist (Rho et al., 2018; McCarthy et al., 2019) especially with the growth in telescopic power most notably signified in the upcoming launch of the *James Webb Space Telescope (JWST)*.

2 Computational Details

Precise optimization of the reference geometry is the first step to computing QFF-based anharmonic rovibrational data. The geometry optimization and all subsequent energy computations use CCSD(T)-F12b with the cc-pVTZ-F12 (Hill & Peterson, 2010; Prascher et al., 2011) basis set (abbreviated as F12-TZ from here on) in MOLPRO2015.1 (Werner et al., 2015, 2012). The optimized geometry is then used to compute the harmonic vibrational frequencies within MOLPRO for comparison to those that result from the QFF. From the reference geometry of each silicon oxide molecule, coordinates are constructed to define the QFF with the bond lengths displaced by 0.005 Å and the bond angles and dihedrals displaced by 0.005 radians. Each of the four molecules has its own unique coordinate system since each has a different number of bond lengths, angles, and dihedrals giving different numbers of total points necessary for the QFF. SiO_2 has 57; SiO_3 has 413; Si_2O_3 has 1585; and Si_2O_4 has 1973 points. The coordinates for each system are defined below with atom labels in Figure 1. The out-of-plane torsional modes are labeled as OPB. The coordinates for SiO_2:

$$S_1(\sigma_g) = \frac{1}{\sqrt{2}}[(Si - O_A) + (Si - O_B)] \quad (1)$$

$$S_2(\sigma_u) = \frac{1}{\sqrt{2}}[(Si - O_A) - (Si - O_B)] \quad (2)$$

$$S_3(\pi_u) = \angle(O_A - Si - O_B) \quad (3)$$

$$S_4(\pi_u) = \angle(O_A - Si - O_B); \quad (4)$$

SiO_3

$$S_1(a_1) = Si - O_A \quad (5)$$
$$S_2(a_1) = \frac{1}{\sqrt{2}}[(O_B - Si) + (O_C - Si)] \quad (6)$$
$$S_3(a_1) = \frac{1}{\sqrt{2}}[\angle(O_B - Si - O_A) + \angle(O_C - Si - O_A)] \quad (7)$$
$$S_4(b_2) = \frac{1}{\sqrt{2}}[(O_B - Si) - (O_C - Si)] \quad (8)$$
$$S_5(b_2) = \frac{1}{\sqrt{2}}[\angle(O_B - Si - O_A) - \angle(O_C - Si - O_A)] \quad (9)$$
$$S_6(b_1) = OPB(O_A - Si - O_B - O_C); \quad (10)$$

Si_2O_3

$$S_1(a_1) = Si_1 - Si_2 \quad (11)$$
$$S_2(a_1) = \frac{1}{\sqrt{2}}[(O_A - Si_A) + (O_A - Si_B)] \quad (12)$$
$$S_3(a_1) = \frac{1}{\sqrt{2}}[(Si_A - O_B) + (Si_B - O_C)] \quad (13)$$
$$S_4(a_1) = \frac{1}{\sqrt{2}}[\angle(O_B - Si_A - O_A) + \angle(O_C - Si_B - O_A)] \quad (14)$$
$$S_5(b_2) = \frac{1}{\sqrt{2}}[(O_A - Si_A) - (O_A - Si_B)] \quad (15)$$
$$S_6(b_2) = \frac{1}{\sqrt{2}}[(Si_A - O_B) - (Si_B - O_C)] \quad (16)$$
$$S_7(b_2) = \frac{1}{\sqrt{2}}[\angle(O_B - Si_A - O_A) - \angle(O_C - Si_B - O_A)] \quad (17)$$
$$S_8(b_1) = \frac{1}{\sqrt{2}}[\tau(O_B - Si_A - O_A - Si_B) - \tau(O_C - Si_B - O_A - Si_A)] \quad (18)$$
$$S_9(a_2) = \frac{1}{\sqrt{2}}[\tau(O_B - Si_A - O_A - Si_B) + \tau(O_C - Si_B - O_A - Si_A)]; \quad (19)$$

and Si_2O_4

$$S_1(a_g) = \frac{1}{\sqrt{2}}[(O_A - O_B) + (Si_A - Si_B)] \quad (20)$$
$$S_2(a_g) = \frac{1}{\sqrt{2}}[(O_A - O_B) - (Si_A - Si_B)] \quad (21)$$
$$S_3(a_g) = \frac{1}{\sqrt{2}}[(Si_A - O_C) + (Si_B - O_D)] \quad (22)$$
$$S_4(b_{1u}) = \frac{1}{2}[(O_A - Si_A) - (O_A - Si_B) - (O_B - Si_A) + (O_B - Si_B)] \quad (23)$$
$$S_5(b_{1u}) = \frac{1}{2}[\angle(O_C - Si_A - O_A) - \angle(O_C - Si_A - O_B) - \angle(O_D - Si_2 - O_A) + \angle(O_D - Si_B - O_B)] \quad (24)$$
$$S_6(b_{2u}) = \frac{1}{2}[(O_A - Si_A) + (O_A - Si_B) - (O_B - Si_A) - (O_B - Si_B)] \quad (25)$$
$$S_7(b_{2u}) = \frac{1}{2}[\angle(O_C - Si_A - O_A) + \angle(O_C - Si_A - O_B) - \angle(O_D - Si_2 - O_A) - \angle(O_D - Si_B - O_B)] \quad (26)$$
$$S_8(b_{3g}) = \frac{1}{\sqrt{2}}[(Si_A - O_C) - (Si_B - O_D)] \quad (27)$$
$$S_9(b_{3g}) = \frac{1}{2}[(O_A - Si_A) - (O_A - Si_B) + (O_B - Si_A) - (O_B - Si_B)] \quad (28)$$
$$S_{10}(b_{3u}) = \frac{1}{\sqrt{2}}[(O_C)_z + (O_D)_z] \quad (29)$$
$$S_{11}(b_{3u}) = \frac{1}{2}[(O_A)_z + (O_B)_z - (Si_A)_z - (Si_B)_z] \quad (30)$$
$$S_{12}(b_{2u}) = \frac{1}{\sqrt{2}}[(O_C)_z - (O_D)_z], \quad (31)$$

where the last of these three has exhibited some questionable results in the low-frequency range for the magnesium fluoride dimer (Palmer & Fortenberry, 2018). The other coordinate systems have been utilized successfully in previous studies on the magnesium hydride monomer, $HeHHe^+$, carbon dioxide, CO_3, $NCNCN^-$, and C_2O_3 (Palmer & Fortenberry, 2018; Stephan & Fortenberry, 2017; Fortenberry et al., 2019; Dubois et al., 2019).

The resulting energies are fit to a least-squares polynomial giving a sum of squared residuals on the order of 10^{-17} a.u.^{2} for all molecules but Si_2O_4 which is 10^{-13} a.u.^{2} This fit determines the actual minimum, or equilibrium, geometry. The final set of force constants are generated by refitting the points to this new minimum; these are given in the supplemental information (SI). The INTDER program (Allen & coworkers, 2005) transforms these force constants into Cartesian coordinates for more general implementation. Then, the SPECTRO program (Gaw et al., 1991) computes the harmonic and anharmonic frequencies including anharmonic zero-point vibrational energies (ZPVEs) using

Table 1. The F12-TZ Geometrical Parameters (in Å or Degrees) as Defined from Figure 1.

	SiO_2	SiO_3	Si_2O_3	Si_2O_4
r_0 (Si_A−O_A)	1.51249	1.50567	1.50675	1.50045
r_0 (Si_A−O_B)		1.62024	1.67351	1.66525[a]
$\angle_0$(O_A−Si_A−O_B)		148.675	137.445	90.544
r_0 (Si_A−Si_B)			2.21681	2.36644
$\angle_0$(O_A−Si_A−O_C)				135.326
r_e (Si_A−O_A)	1.51066	1.50395	1.50726	1.50337
r_e (Si_A−O_B)		1.61659	1.66903	1.66135[a]
$\angle_e$(O_A−Si_A−O_B)		148.814	137.313	90.673
r_e (Si_A−Si_B)			2.21069	2.36327
$\angle_e$(O_A−Si_A−O_C)				135.337

[a]This is actually the r_0 (Si_A−O_C), but is placed here for consistency of bond type.

vibrational perturbation theory at second-order (VPT2) as well as spectroscopic constants making use of rotational perturbation theory at second-order (Mills, 1972; Watson, 1977; Papousek & Aliev, 1982) and Fermi resonance polyads (Martin & Taylor, 1997).

The B3LYP/aug-cc-pVDZ double-harmonic intensities and dipole moments are computed with Gaussian09 (Becke, 1993; Yang et al., 1986; Lee et al., 1988; Dunning, 1989; Frisch et al., 2009). These have been shown to be in good agreement with higher-level computations previously (Yu et al., 2015; Finney et al., 2016). Additionally, the scaling factors for the Si-O stretching (0.98242) and bending (0.99261) frequencies determined previously (Westbrook & Fortenberry, 2020) are applied to the harmonics computed directly in MOLPRO for comparison of their performance in these related but not identical systems.

3 Results & Discussion

The geometries for each of the four molecules examined here are given in Table 1 with labels from Figure 1. Most notably, the Si_A−O_A bond lengths, those that have the oxygen atom in a silaketone moiety (external Si=O group) are largely consistent with a bond length on the order of 1.5 Å. SiO_2 is the exception to this where the longer bond length likely arises from the weakening of the silicon atom's electron donation due to having two Si=O bonds instead of just one, and its magnitude here is in line with that computed previously (Tremblay et al., 1996). The Si_A−$O_{B/C}$ bonds can be thought of as single bonds from a carbon analogue (Fortenberry et al., 2019) and are notably and consistently longer. The Si−Si bonds are longer in Si_2O_4 than in Si_2O_3, but the additional oxygen atom in the former naturally increases the size of the ring thus making for a longer diagonal distance between silicon atoms.

3.1 Anharmonic Frequencies

The F12-TZ vibrational frequencies for SiO_2 are given in Table 2. While the gas phase values for this molecule are not known, the argon matrix results correlate exceptionally well with the explicit QFF values for the 1420.7 cm^{-1} and 289.0 cm^{-1} fundamentals compared to the 1416 cm^{-1} and 273 cm^{-1} experimental frequencies (Jacox, 1994). Interestingly, the scaled 1414.4 cm^{-1} and 288.5 cm^{-1} frequencies for the same modes are in slightly closer agreement with experiment. Even so, the difference in the explicit QFF anharmonic frequencies and the scaled values are within the accuracy (7 cm^{-1}) of the F12-TZ approach implying that either is a valuable choice of method. The vibrationally-

Table 2. The F12-TZ Vibrational Frequencies (in cm^{-1}) and Intensities (in km/mol) for SiO_2.

Mode	Description	Symmetry	Frequency	Exp.[a]	Scaled	Δ(QFF-Scaled)
ω_1	Si−O antisymm. stretch	(σ_u)	1439.7 (67)			
ω_2	Si−O symm. stretch	(σ_g)	992.4 (0)			
ω_3	O−Si−O bend	(π_u)	290.6 (79)			
ZPVE			1501.9			
ν_1	Si−O antisymm. stretch	(σ_u)	1420.7	1416	1414.4	6.3
ν_2	Si−O symm. stretch	(σ_g)	984.2		975.0	9.2
ν_3	O−Si−O bend	(π_u)	289.0	273	288.5	0.5

[a]Argon matrix experimental data from (H. Schnöckel, 1978; V. H. Schnöckel, 1980; Andrews & McCluskey, 1992; Jacox, 1994)

Table 3. The F12-TZ QFF Vibrational Frequencies (cm^{-1}) and Intensities (km/mol) for C_{2v} SiO_3.

Mode	Description	Symmetry	Frequency	Exp.[a]	Scaled	Δ(QFF-Scaled)
ω_1	Si-O_A	a_1	1391.4 (114)			
ω_2	Si-O_B + Si-O_C	a_1	894.2 (5)			
ω_3	Si-O_B - Si-O_C	b_2	868.5 (90)			
ω_4	∠ O_A-Si-O_B + ∠ O_A-Si-O_C	a_1	515.0 (25)			
ω_5	Si OPB	b_1	309.7 (82)			
ω_6	∠ O_A-Si-O_B - ∠ O_A-Si-O_C	b_2	299.3 (60)			
ZPVE			2129.5			
ν_1	Si-O_A	a_1	1371.0	1363.5 (100)	1366.9	4.1
ν_2	Si-O_B + Si-O_C	a_1	885.3	877.1 (12)	878.5	6.8
ν_3	Si-O_B - Si-O_C	b_2	857.1	855.3 (53)	853.2	3.9
ν_4	∠ O_A-Si-O_B + ∠ O_A-Si-O_C	a_1	497.0	–	511.2	-14.2
ν_5	Si OPB	b_1	305.3	287.8 (96)	307.4	-2.1
ν_6	∠ O_A-Si-O_B - ∠ O_A-Si-O_C	b_2	298.0	292.0 (62)	297.1	0.9

[a]Argon matrix data from (Tremblay et al., 1996).

dark symmetric stretch has a larger difference between the two anharmonic frequencies, but no experimental data can verify which is more accurate. The F12-TZ QFF produces nearly identical values as gas-phase experimental CO_2 frequencies (differences of less than 2 cm^{-1} in every case) (Fortenberry et al., 2019), and similar accuracies appear to be present in the silicon analogue, as well.

The strong correspondence between theory and argon matrix experiments continues with C_{2v} SiO_3. As shown in Table 3, the difference between the F12-TZ SiO_3 anharmonic frequencies and that for the argon matrix experiments(Tremblay et al., 1996) is never more than 8 cm^{-1}, and ν_3 at 857.1 cm^{-1} is within 2 cm^{-1} of experiment. Granted, the matrix will shift these values relative to the gas phase values that would be observed in astrophysical contexts, but, again, these shifts should be small. Furthermore, the B3LYP/aug-cc-pVTZ double-harmonic intensities are in at least semi-quantitative agreement with experiment showing which bands could be considered strong and which could be considered weak. Unsurprisingly, the ν_1 terminal Si=O_A stretch at 1371.0 cm^{-1} is the brightest vibrational mode, and the OPB bend for O_A is also bright lining up with experiment.

Table 4. Si_2O_3 F12-TZ Harmonic and Fundamental Vibrational Frequencies (in cm^{-1}) and B3LYP Intensities (in km/mol).

Mode	Description	Symmetry	Frequency	Scaled	Δ(QFF-Scaled)
ω_1	Si_A-O_B + Si_B-O_C	a_1	1331.0 (17)		
ω_2	Si_A-O_B - Si_B-O_C	b_2	1274.0(152)		
ω_3	Si_A-O_A + Si_B-O_A	a_1	859.1(122)		
ω_4	Si_A-O_A - Si_B-O_A	b_2	663.2(52)		
ω_5	Si_A-Si_B	a_1	440.7(21)		
ω_6	∠ O_A-Si_A-O_B - ∠ O_A-Si_B-O_C	b_2	248.7(16)		
ω_7	τ(O_B-Si_A-O_A-Si_B) + τ(O_C-Si_B-O_A-Si_A)	b_1	245.7(62)		
ω_8	∠ O_A-Si_A-O_B + ∠ O_A-Si_B-O_C	a_1	189.8(30)		
ω_9	τ(O_B-Si_A-O_A-Si_B) + τ(O_C-Si_B-O_A-Si_A)	a_2	153.4(0)		
ZPVE			2679.5		
ν_1	Si_A-O_B + Si_B-O_C	a_1	1303.3	1307.6	-4.3
ν_2	Si_A-O_B - Si_B-O_C	b_2	1245.6	1251.6	-6.0
ν_3	Si_A-O_A + Si_B-O_A	a_1	836.2	844.0	-7.8
ν_4	Si_A-O_A - Si_B-O_A	b_2	637.6	651.6	-14.0
ν_5	Si_A-Si_B	a_1	432.5	437.5	-5.0
ν_6	∠ O_A-Si_A-O_B - ∠ O_A-Si_B-O_C	b_2	245.0	246.9	-1.9
ν_7	τ(O_B-Si_A-O_A-Si_B) + τ(O_C-Si_B-O_A-Si_A)	b_1	244.6	243.9	0.7
ν_8	∠ O_A-Si_A-O_B + ∠ O_A-Si_B-O_C	a_1	188.2	188.4	-0.2
ν_9	τ(O_B-Si_A-O_A-Si_B) + τ(O_C-Si_B-O_A-Si_A)	a_2	153.7	152.3	1.4

The previous SiO_3 experiment could not identify the a_1 ν_4 symmetric bend (equivalently described as the O−O stretch). This fundamental has an intensity greater than the ν_2 Si−O symmetric stretch previously characterized in the argon matrix experiments (Tremblay et al., 1996). The reason is likely that the previous DFT computations suggested that the fundamental should lie higher in frequency close to 582 cm^{-1}. However, the present work strongly suggests that this fundamental is much lower in frequency at 497.0 cm^{-1}. Unfortunately, this region of the IR spectrum is not reported in this previous work negating any *ex post facto* analysis. Regardless, the F12-TZ QFF values confirm the other argon matrix fundamental vibrational frequency assignments for C_{2v} SiO_3(Tremblay et al., 1996) and show that the last remaining band is most likely lower in frequency than previously believed.

The F12-TZ QFF fundamental vibrational frequencies for Si_2O_3 have not been previously explored experimentally or theoretically and are given here in Table 4. The silaketone stretches (ν_1 and ν_2) are in the same frequency range as that for SiO_3, and the antisymmetric ν_2 stretch at 1245.6 cm^{-1} has the greatest intensity of all the fundamentals. This is also true for the related C_2O_3 and $C_2N_3^-$ molecules (Fortenberry et al., 2019; Dubois et al., 2019). The a_1 ν_3 stretching of the central O_A atom produces the next-brightest fundamental at 836.2 cm^{-1}. The permanent dipole moment is being extended in this case, giving a larger charge separation upon vibration. The remaining frequencies are dimmer but still non-negligible, and the five lowest frequency fundamentals are all below 500 cm^{-1}, as is common for such heavy atoms like silicon (Kloska & Fortenberry, 2018; Palmer & Fortenberry, 2018; Valencia et al., 2020).

The 12 fundamental vibrational frequencies for D_{2h} Si_2O_4 are given in Table 5. The silaketone stretches are blue-shifted in this molecule compared to Si_2O_3 and are present above 1300 cm^{-1}. The b_{3g} ν_2 antisymmetric stretch, again, has the largest intensity of

Table 5. Si_2O_4 F12-TZ Harmonic and Fundamental Vibrational Frequencies (in cm^{-1}) and B3LYP Intensities (in km/mol).

Mode	Description	Symmetry	Frequency	Exp.[a]	Scaled	Δ(QFF-Scaled)
ω_1	Si_A-O_C + Si_B-O_D	a_g	1354.4 (0)			
ω_2	Si_A-O_C - Si_B-O_D	b_{3g}	1316.9 (382)			
ω_3	Si_A-O_B + Si_B-O_B - Si_A-O_A - Si_B-O_A	b_{2u}	904.8 (259)			
ω_4	O_A-O_B + Si_A-Si_B	a_g	871.6 (0)			
ω_5	O_B-Si_A - O_B-Si_B + O_A-Si_A - O_A-Si_B	b_{3g}	804.0 (252)			
ω_6	O_B-Si_A - O_B-Si_B - O_A-Si_A + O_A-Si_B	b_{1u}	718.7 (0)			
ω_7	O_A-O_B - Si_A-Si_B	a_g	488.0 (0)			
ω_8	Symm. O_A-O_B OPB	b_{3u}	465.4 (99)			
ω_9	O_C-Si_A-O_B - O_C-Si_A-O_A + O_D-Si_B-O_B + O_D-Si_B-O_A	b_{1u}	313.3 (0)			
ω_{10}	O_C-Si_A-O_B - O_C-Si_A-O_A + O_D-Si_B-O_B - O_D-Si_B-O_A	b_{2u}	295.5† (43)			
ω_{11}	Antisymm. O_C/O_D OPB	b_{2u}	236.6 (0)			
ω_{12}	Symm. O_C/O_D OPB	b_{3u}	121.5† (26)			
ZPVE			3796.3			
ν_1	Si_A-O_C + Si_B-O_D	a_g	1338.2		1330.6	7.6
ν_2	Si_A-O_C - Si_B-O_D	b_{3g}	1303.6	1293.3	1293.7	9.9
ν_3	Si_A-O_B + Si_B-O_B - Si_A-O_A - Si_B-O_A	b_{2u}	911.7	889.2	888.9	22.8
ν_4	O_A-O_B + Si_A-Si_B	a_g	861.3		856.3	5.0
ν_5	O_B-Si_A - O_B-Si_B + O_A-Si_A - O_A-Si_B	b_{3g}	856.8	786.4	789.9	66.9
ν_6	O_B-Si_A - O_B-Si_B - O_A-Si_A + O_A-Si_B	b_{1u}	658.1		706.1	-48.0
ν_7	O_A-O_B - Si_A-Si_B	a_g	485.9		479.4	6.5
ν_8	Symm. O_A-O_B OPB	b_{3u}	456.1		462.0	-5.9
ν_9	O_C-Si_A-O_B - O_C-Si_A-O_A + O_D-Si_B-O_B + O_D-Si_B-O_A	b_{1u}	281.7		311.0	-29.3
ν_{10}	O_C-Si_A-O_B - O_C-Si_A-O_A + O_D-Si_B-O_B - O_D-Si_B-O_A	b_{2u}			293.3	
ν_{11}	Antisymm. O_C/O_D OPB	b_{2u}	230.5		234.9	-4.4
ν_{12}	Symm. O_C/O_D OPB	b_{3u}			120.6	

[a] Argon matrix experimental results from (Mehner et al., 1980). † Denotes a MOLPRO harmonic frequency

all the fundamental frequencies for this molecule. Stretches within the ring (ν_3 and ν_5) are the next-brightest with intensities above 250 km/mol, more than 3.5 times that of the antisymmetric stretch in water. Comparison to argon matrix data from (Mehner et al., 1980) gives good agreement between the 1293.3 cm^{-1} value and the F12-TZ QFF ν_2 frequency at 1303.6 cm^{-1}. This deteriorates slightly for ν_3 where experiment places this at 889.2 cm^{-1} and the QFF is 911.7 cm^{-1}. The correlation is completely off for ν_5 with experiment attributing this ring deformation to a band at 786.4 cm^{-1} and the QFF at 856.8 cm^{-1}. Either the band has been misassigned in the experiment, or the computations are off.

In this case, the latter is most likely correct. The fitting of the points was the worst for Si_2O_4 of the silicon oxides studied. Furthermore, two harmonic vibrational frequencies computed via the QFF do not align with those computed from within MOLPRO's standard harmonic frequency computation, ω_{10} and ω_{12}. The OPB coordinate struggles to define the proper motion within the constraints of the QFF and VPT2, and this subsequently affects the fitting of the force constants for the other coordinates. The potential for the OPB is likely flat reducing the capabilities of VPT2 as defined by the QFF. The ν_{10} and ν_{12} fundamentals could not even be computed from the QFF data. Hence, the F12-TZ QFF VPT2 anharmonic vibrational frequencies for Si_2O_4 below the silaketone stretches should be treated as suggestions.

However, all is not lost in the prediction of these anharmonic frequencies. The recent determination of scaling factors for M−O stretches and bends (where M is a second-row atom) can be applied to Si_2O_4. Doing so actually produces a fundamental frequency for ν_3 at 888.9 $cm^{-1}$and ν_5 at 789.9 cm^{-1}. Both are within 3.5 cm^{-1} of the argon matrix experiment. Furthermore, the ν_2 antisymmetric stretch is 1293.7 cm^{-1} from the scaled values, 9.9 cm^{-1} below the explicit QFF, and only 0.4 cm^{-1} below the experimental value. Consequently, the scaled harmonics are likely producing more meaningful fundamental vibrational frequencies for this molecule than the QFF. The harmonic force field is much better behaved and less likely to suffer from noise contamination in these numerical derivatives (Huang & Lee, 2008, 2009), and the amount of absolute anharmonicity is relatively small in the first place.

The scaled harmonic frequencies are also listed for the other three molecules giving slightly better correlation with experiment for SiO_2 (Table 2) as discussed previously. Agreement between experiment and scaled harmonics of SiO_3 (Table 3) is comparable with the F12-TZ QFF VPT2 results. Some modes are better with the scaled values (ν_1) and some with the explicit anharmonicity computed (ν_3) implying that either is appropriate. Both also demonstrate that ν_4 is still lower in frequency than previous experiments explored. Since there are no experimental data for Si_2O_3, comparison between the QFF VPT2 results and the scaled harmonics both with F12-TZ is necessary, but both are quite comparable with one another (Table 4). All modes agree to within 8 cm^{-1} save for the b_2 ν_4 antisymmetric stretch. The mean absolute error (MAE) between the QFF and scaled harmonics for the stretching frequencies is 5.8 cm^{-1} when removing ν_4 and 8.0 cm^{-1} when including it. The bends and torsions are much closer with the MAE at 1.8 cm^{-1}, but, again, the magnitudes of the frequencies are smaller in the first place. Hence, these scaling factors are comparable to the QFF VPT2 fundamental vibrational frequencies implying that these heuristics could be used as a first-order guess to the fundamental vibrational frequencies of Si_2O_4 and potentially even for larger silicon oxide clusters where QFFs or any anharmonic vibrational frequency computations are prohibitively large.

3.2 Rotational and Spectroscopic Constants

The spectroscopic constants for each of the molecules examined are given in Table 6. These include the pure rotational constants, the vibrationally-averaged rotational constants, the quartic and sextic (Watson S Hamiltonian) distortion constants, and even

Table 6. The F12-TZ QFF Spectroscopic Data for the Four Silicon Oxides.

	SiO_2	SiO_3	Si_2O_3	Si_2O_4
A_0 (MHz)		22360.3	21364.6	11474.0
B_0 (MHz)	6907.7	5489.9	1766.6	1636.1
C_0 (MHz)		4400.5	1630.8	1433.1
A_1 (MHz)		22333.1	21390.3	11469.1
B_1 (MHz)	6872.3	5466.1	1761.6	1632.6
C_1 (MHz)		4384.4	1626.6	1430.4
A_2 (MHz)		22292.4	21361.1	11465.8
B_2 (MHz)	6888.1	5480.1	1762.9	1633.0
C_2 (MHz)		4392.0	1627.6	1430.8
A_3 (MHz)		22446.5	21282.1	11497.3
B_3 (MHz)	6920.3	5469.6	1764.8	1633.3
C_3 (MHz)		4391.4	1628.1	1430.4
A_4 (MHz)		22001.5	20997.0	11458.5
B_4 (MHz)		5518.5	1768.1	1635.0
C_4 (MHz)		4392.3	1629.6	1431.8
A_5 (MHz)		22310.3	21576.9	11442.8
B_5 (MHz)		5493.9	1761.6	1635.2
C_5 (MHz)		4409.0	1627.2	1431.5
A_6 (MHz)		22408.0	21370.4	11446.5
B_6 (MHz)		5504.1	1768.2	1633.6
C_6 (MHz)		4400.9	1631.2	1430.7
A_7 (MHz)			21368.9	
B_7 (MHz)			1767.8	
C_7 (MHz)			1632.6	
A_8 (MHz)			21507.1	
B_8 (MHz)			1767.9	
C_8 (MHz)			1630.7	
A_9 (MHz)			21279.8	
B_9 (MHz)			1768.2	
C_9 (MHz)			1633.4	
Δ_J (Hz)	1.500	941.78	120.62	56.658
Δ_K (kHz)		133.62	363.47	9.985
Δ_{JK} (kHz)		15.616	-4.444	0.389
δ_J (Hz)		227.57	18.119	8.426
δ_K (kHz)		11.708	1.065	0.484
Φ_J (μHz)	-8.885	518.99	2.540	2.770
Φ_K (Hz)		-0.240	9.387	0.022
Φ_{JK} (mHz)		80.382	0.920	0.242
Φ_{KJ} (mHz)		-233.60	-127.77	-4.098
ϕ_j (μHz)		261.21	4.481	1.058
ϕ_{jk} (mHz)		45.749	0.152	0.152
ϕ_k (Hz)		1.292	0.502	0.009
μ (D)	–	0.87	0.66	–

the dipole moments of the two C_{2v} molecules. While these may not be as accurate as methods including core electron correlation or other additive factors (Agbaglo & Fortenberry, 2019a, 2019b), these rotational constants should serve as a good starting point for assessing the rotational spectra of these molecules. Strangely, a search of the literature did not yield any experimental rotational constants for SiO_2 which are provided here for this nonpolar molecule. The other three molecules are all clearly near-prolate rotors especially for Si_2O_3.

The vibrationally-excited rotational constants (numbered in the same order as the fundamental vibrational frequencies) for Si_2O_4 are given for the modes with the least questionable vibrational frequencies. While the pure rotational transitions of this molecule will not be observed since it has no dipole moment, the A_2, B_2, and C_2 values, however, will likely be important for rovibrational modeling since ν_2 of this molecule has the largest infrared intensity computed of the set. Finally, the dipole moments are reported at the bottom of Table 6. SiO_3 is the most polar, but Si_2O_3 has a smaller but similar magnitude dipole moment. This differs from the carbon analogues where C_2O_3 is almost apolar (Fortenberry et al., 2019) likely due to the larger electronegativity difference bewtween oxygen and silicon as well as the longer Si−O bonds.

4 Conclusions

The small silicon oxide clusters SiO_2, SiO_3, Si_2O_3, and Si_2O_4 are shown here to be stable species with notably bright mid- to far-IR active fundamental vibrational frequencies. The antisymmetric silaketone stretch in the silicon dioxide dimer has the largest intensity of the set. The range between 1420 cm^{-1} and 1250 cm^{-1} (7.0 μm and 8.0 μm) contains this most intense band and its counterparts from the other three oxides. The other infrared bands typically fall below 700 cm^{-1} (>14.3 μm) with many of the silicon oxides analyzed here having one or two bands around 850 cm^{-1} (∼11.8 μm). Each of these regions have notable bumps from astronomical spectra (Molster et al., 2001), implying that small, geochemically-relevant silicon oxides may be present in circumstellar media and protoplanetary disks. Upcoming *JWST* spectra could potentially resolve such peaks. The polar SiO_3 and Si_2O_3 clusters could be observed from the ground with radiotelescopes, and the present data will aid in the experimental characterization necessary to provide reference data for such observations.

Additionally, the previously derived scaling factors (Westbrook & Fortenberry, 2020) show promise in treating similar inorganic oxides that are intractable for QFF computations. Comparison to experimental spectra for SiO_2 and SiO_3 shows that both the explicit anharmonic computations and the scaled harmonics are similarly accurate partly due to the small magnitudes of the anharmonicities of the molecules examined. However, these scaled harmonics also do not suffer from coordinate issues observed in Si_2O_4 making them also potentially useful for future exploration of larger mineralogically-relevant inorganic oxides.

Acknowledgements

The authors acknowledge funding from the NSF (OIA-1757220), NASA (NNX17AH15G), and the University of Mississippi start-up funds. Datasets for this research are included in this paper (and its supplementary information files).

References

Adler, T. B., Knizia, G., & Werner, H.-J. (2007). A simple and efficient CCSD(T)-F12 approximation. *J. Chem. Phys.*, *127*, 221106.

Agbaglo, D., & Fortenberry, R. C. (2019a). The performance of CCSD(T)-F12/aug-

cc-pVTZ for the computation of anharmonic fundamental vibrational frequencies. *Int. J. Quantum Chem.*, *119*, e25899.

Agbaglo, D., & Fortenberry, R. C. (2019b). The performance of explicitly correlated wavefunctions [CCSD(T)-F12b] in the computation of anharmonic vibrational frequencies. *Chem. Phys. Lett.*, *734*, 136720.

Agbaglo, D., Lee, T. J., Thackston, R., & Fortenberry, R. C. (2019). A small molecule with pah vibrational properties and a detectable rotational spectrum: *c*-(C)C_3H_2, cyclopropenylidenyl carbene. *Astrophys. J.*, *871*, 236.

Allen, W. D., & coworkers. (2005). (*INTDER* 2005 is a General Program Written by W. D. Allen and Coworkers, which Performs Vibrational Analysis and Higher-Order Non-Linear Transformations.)

Andrews, L., & McCluskey, M. (1992). Bending modes of SiO_2 and GeO_2 in solid argon. *J. Mol. Spectrosc.*, *154*, 223-225.

Becke, A. D. (1993). Density-functional thermochemistry. iii. the role of exact exchange. *J. Chem. Phys.*, *98*, 5648-5652.

Beste, A., & Bartlett, R. J. (2002). The electronic structure of SiO_3: A problematic example for coupled cluster methods. *Chem. Phys. Lett.*, *366*, 100-108.

Bizzocchi, L., Lattanzi, V., Laas, J., Spezzano, S., Giuliano, B. M., Prudenzano, D., ... Caselli, P. (2017). Accurate sub-millimetre rest frequencies for $HOCO^+$ and $DOCO^+$ ions. *Astron. Astrophys.*, *602*, A34.

Dubois, D., Sciamma-O'Brien, E., & Fortenberry, R. C. (2019). The fundamental vibrational frequencies and spectroscopic constants of the dicyanoamine anion, ncncn$^-$ ($c_2n_3^-$): Quantum chemical analysis for astrophysical and planetary environments. *Astrophys. J.*, *883*, 109.

Dunning, T. H. (1989). Gaussian basis sets for use in correlated molecular calculations. i. the atoms boron through neon and hydrogen. *J. Chem. Phys.*, *90*, 1007-1023.

Finney, B., Fortenberry, R. C., Francisco, J. S., & Peterson, K. A. (2016). A spectroscopic case for SPSi detection: The third-row in a single molecule. *J. Chem. Phys.*, *145*, 124311.

Fortenberry, R. C. (2017). Quantum astrochemical spectroscopy. *Int. J. Quant. Chem.*, *117*, 81-91.

Fortenberry, R. C. (2020). The case for gas-phase astrochemistry without carbon. *Mol. Astrophys.*, *18*, 100062.

Fortenberry, R. C., Huang, X., Crawford, T. D., & Lee, T. J. (2014). Quartic force field rovibrational analysis of protonated acetylene, $C_2H_3^+$, and its isotopologues. *J. Phys. Chem. A*, *118*, 7034-7043.

Fortenberry, R. C., Huang, X., Francisco, J. S., Crawford, T. D., & Lee, T. J. (2011a). The *trans*-HOCO radical: Fundamental vibrational frequencies, quartic force fields, and spectroscopic constants. *J. Chem. Phys.*, *135*, 134301.

Fortenberry, R. C., Huang, X., Francisco, J. S., Crawford, T. D., & Lee, T. J. (2011b). Vibrational frequencies and spectroscopic constants from quartic force fields for *cis*-HOCO: The radical and the anion. *J. Chem. Phys.*, *135*, 214303.

Fortenberry, R. C., Huang, X., Francisco, J. S., Crawford, T. D., & Lee, T. J. (2012). Fundamental vibrational frequencies and spectroscopic constants of $HOCS^+$, $HSCO^+$, and isotopologues via quartic force fields. *J. Phys. Chem. A.*, *116*, 9582-9590.

Fortenberry, R. C., & Lee, T. J. (2019). Computational vibrational spectroscopy for the detection of molecules in space. *Ann. Rep. Comput. Chem.*, *15*, 173-202.

Fortenberry, R. C., Lee, T. J., & Müller, H. S. P. (2015). Excited vibrational level rotational constants for SiC_2: A sensitive molecular diagnostic for astrophysical conditions. *Molec. Astrophys.*, *1*, 13-19.

Fortenberry, R. C., Peters, D., Ferari, B. C., & Bennett, C. J. (2019). Rovibrational spectral analysis of CO_3 and C_2O_3: Potential sources for O_2 observed in comet

67P/Churyumov-Gerasimenko. *Astrophys. J. Lett.*, *886*, L10.

Frisch, M. J., Trucks, G. W., Schlegel, H. B., Scuseria, G. E., Robb, M. A., Cheeseman, J. R., ... Fox, D. J. (2009). *Gaussian 09 Revision D.01.* (Gaussian Inc. Wallingford CT)

Gaw, J. F., Willets, A., Green, W. H., & Handy, N. C. (1991). SPECTRO: A program for the derivation of spectrscopic constants from provided quartic force fields and cubic dipole fields. In J. M. Bowman & M. A. Ratner (Eds.), *Advances in molecular vibrations and collision dynamics* (p. 170-185). Greenwich, Connecticut: JAI Press, Inc.

Hill, J. G., & Peterson, K. A. (2010). Correlation consistent basis sets for explicitly correlated wavefunctions: Valence and core-valence basis sets for Li, Be, Na, and Mg. *Phys. Chem. Chem. Phys.*, *12*, 10460-10468.

Huang, X., Fortenberry, R. C., & Lee, T. J. (2013). Protonated nitrous oxide, $NNOH^+$: Fundamental vibrational frequencies and spectroscopic constants from quartic force fields. *J. Chem. Phys.*, *139*(8), 084313.

Huang, X., & Lee, T. J. (2008). A procedure for computing accurate *ab initio* quartic force fields: Application to HO_2^+ and H_2O. *J. Chem. Phys.*, *129*, 044312.

Huang, X., & Lee, T. J. (2009). Accurate *ab initio* quartic force fields for NH_2^- and CCH^- and rovibrational spectroscopic constants for their isotopologs. *J. Chem. Phys.*, *131*, 104301.

Huang, X., Taylor, P. R., & Lee, T. J. (2011). Highly accurate quartic force field, vibrational frequencies, and spectroscopic constants for cyclic and linear $C_3H_3^+$. *J. Phys. Chem. A*, *115*, 5005-5016.

Jacox, M. E. (1994). Vibrational and electronic energy levels of polyatomic transient molecules. *J. Phys. Chem. Ref. Data*, *23*, 1-461.

Kitchens, M. J. R., & Fortenberry, R. C. (2016). The rovibrational nature of closed-shell third-row triatomics: HOX and HXO, X = Si^+, P, S^+, and Cl. *Chem. Phys.*, *472*, 119-127.

Kloska, K. A., & Fortenberry, R. C. (2018). Gas-phase spectra of MgO molecules: A possible connection from gas-phase molecules to planet formation. *Mon. Not. Royal Astron. Soc.*, *474*, 2055-2063.

Knizia, G., Adler, T. B., & Werner, H.-J. (2009). Simplified CCSD(T)-F12 Methods: Theory and benchmarks. *J. Chem. Phys.*, *130*, 054104.

Lee, C., Yang, W. T., & Parr, R. G. (1988). Development of the colle-salvetti correlation-energy formula into a functional of the electron density. *Phys. Rev. B.*, *37*, 785-789.

Martin, J. M. L., & Taylor, P. R. (1997). Accurate *ab initio* quartic force field for *trans*-hnnh and treatment of resonance polyads. *Spectrochim. Acta A*, *53*, 1039-1050.

McCall, B. J. (2006). Dissociative recombination of cold h_3^+ and its interstellar implications. *Phil. Trans. Royal Soc. A*, *364*, 2953-2963.

McCarthy, M. C., Gottlieb, C. A., & Cernicharo, J. (2019). Building blocks of dust: A coordinated laboratory and astronomical study of the archtype AGB carbon star IRC+10216. *J. Molec. Spectrosc.*, *356*, 7-20.

Mehner, T., Göckes, H. J., Schunck, S., & Schnöckel, H. (1980). Dimeres SiO_2 matrix-ir-untersuchungen und ab initio scf-rechnungen. *Z. Anorg. Allg. Chem.*, *580*, 121-130.

Mills, I. M. (1972). Vibration-rotation structure in asymmetric- and symmetric-top molecules. In K. N. Rao & C. W. Mathews (Eds.), *Molecular spectroscopy - modern research* (p. 115-140). New York: Academic Press.

Molster, F. J., Lim, T. L., Sylvester, R. J., Waters, L. B. F. M., Barlow, M. J., Beintema, D. A., ... Schmitt, B. (2001). The complete iso spectrum of ngc 6302. *Astron. Astrophys.*, *372*, 165-172.

Palmer, C. Z., & Fortenberry, R. C. (2018). Rovibrational considerations for the monomers and dimers of magnesium hydride (MgH_2) and magnesium fluoride

(MgF_2). *J. Phys. Chem. A*, *122*, 7079-7088.

Papousek, D., & Aliev, M. R. (1982). *Molecular vibration-rotation spectra.* Amsterdam: Elsevier.

Prascher, B. P., Woon, D. E., Peterson, K. A., Dunning, T. H., & Wilson, A. K. (2011). Gaussian basis sets for use in correlated molecular calculations. vii. valence, core-valence, and scalar relativistic basis sets for Li, Be, Na, and Mg. *Theor. Chem. Acc.*, *128*, 69-82.

Raghavachari, K., Trucks, G. W., Pople, J. A., & Head-Gordon, M. (1989). A fifth-order perturbation comparison of electron correlation theories. *Chem. Phys. Lett.*, *157*, 479-483.

Rho, J., Gomez, H. L., Boogert, A., Smith, M. W. L., Lagage, P.-O., Dowell, D., ... Cami, J. (2018). A dust twin of Cas A: Cool dust and 21 μm silicate dust feature in the supernova remnant G54.1+0.3. *Mon. Not. Royal Astron. Soc.*, *479*, 5101-5123.

Rouillé, G., Jäger, C., Krasnokutski, S. A., Krebszb, M., & Henning, T. (2014). Cold condensation of dust in the ISM. *Farad. Discuss.*, *168*, 449-460.

Savage, B. D., & Sembach, K. R. (1996). Interstellar abundances from absorption-line observations with the *Hubble Space Telescope*. *Annu. Rev. Astron. Astrophys.*, *34*, 279-329.

Schnöckel, H. (1978). Ir spectroscopic detection of molecular SiO_2. *Angew. Chem. Int. Ed. Engl.*, *17*, 616-617.

Schnöckel, V. H. (1980). Matrixreaktionen von SiO. ir-spektroskopischer nachweis der molekeln SiO_2 und $OSiCl_2$. *Z. Anorg. Allg. Chem.*, *460*, 37-50.

Shavitt, I., & Bartlett, R. J. (2009). *Many-body methods in chemistry and physics: Mbpt and coupled-cluster theory.* Cambridge: Cambridge University Press.

Stephan, C. J., & Fortenberry, R. C. (2017). The interstellar formation and spectra of the noble gas, proton-bound $HeHHe^+$, $HeHNe^+$ and $HeHAr^+$ complexes. *Mon. Not. Royal Astron. Soc.*, *469*, 339-346.

Tremblay, B., Roy, P., Manceron, L., Alikhani, M. E., & Roy, D. (1996). Vibrational spectrum and structure of silicon trioxide SiO_3: A matrix isolation infrared and density functional theory study. *J. Chem. Phys.*, *104*, 2773-2781.

Valencia, E. M., Worth, C. J., & Fortenberry, R. C. (2020). Enstatite ($MgSiO_3$) and forsterite (Mg_2SiO_4) monomers and dimers: Highly-detectable infrared and radioastronomical molecular building blocks. *Mon. Not. Royal Astron. Soc.*, *492*, 276-282.

Wang, L.-S., Desai, S. R., Wu, H., & Nicholas, J. B. (1997). Small silicon oxide clusters: Chains and rings. *Z. Phys. D*, *40*, 36-39.

Wang, L.-S., Wu, H., Desai, S. R., Fan, J., & Colson, S. D. (1996). A photoelectron spectroscopic study of small silicon oxide clusters: SiO_2, Si_2O_3, and Si_2O_4. *J. Phys. Chem.*, *100*, 8697-8700.

Watson, J. K. G. (1977). Aspects of quartic and sextic centrifugal effects on rotational energy levels. In J. R. During (Ed.), *Vibrational spectra and structure* (p. 1-89). Amsterdam: Elsevier.

Werner, H.-J., Knowles, P. J., Knizia, G., Manby, F. R., & Schütz, M. (2012). Molpro: A General-Purpose Quantum Chemistry Program Package. *WIREs Comput. Mol. Sci.*, *2*, 242–253.

Werner, H.-J., Knowles, P. J., Knizia, G., Manby, F. R., Schütz, M., Celani, P., ... Wang, M. (2015). *Molpro, version 2015.1, a package of ab initio programs.* Cardiff, UK. (see http://www.molpro.net)

Westbrook, B. R., & Fortenberry, R. C. (2020). Anharmonic frequencies of $(MO)_2$ and related hydrides for M = Mg, Al, Si, P, S, Ca, & Ti and heuristics for predicting anharmonic corrections of inorganic oxides. *J. Phys. Chem. A.* (*submitted*)

White, W. M. (2013). *Geochemistry* (1st ed.). Hoboken, NJ: Wiley.

Wilson, R. W., Penzias, A. A., Jefferts, K. B., Kutner, M., & Thaddeus, P. (1971). Discovery of interstellar silicon monoxide. *Astrophys. J.*, *167*, L97-L100.

Yang, W. T., Parr, R. G., & Lee, C. T. (1986). Various functionals for the kinetic energy density of an atom or molecule. *Phys. Rev. A*, *34*, 4586-4590.

Yu, Q., Bowman, J. M., Fortenberry, R. C., Mancini, J. S., Lee, T. J., Crawford, T. D., ... Francisco, J. S. (2015). The structure, anharmonic vibrational frequencies, and intensities of $NNHNN^+$. *J. Phys. Chem. A*, *119*, 11623-11631.

Zhao, D., Doney, K. D., & Linnartz, H. (2014). Laboratory gas-phase detection of the cyclopropenyl cation (c-$C_3H_3^+$). *Astrophys. J. Lett.*, *791*, L28.